MICRO-CRACK DEVELOPMENT IN CARBON FIBER BATTERY IN CYCLIC CHARGE/DISCHARGE

A. Pupurs[1,2]*, J. Varna[1]
[1] Department of Engineering Sciences and Mathematics, Luleå University of Technology, Luleå, Sweden
[2] Swerea SICOMP, Piteå, Sweden
* Corresponding author (andrejs.pupurs@ltu.se)

Keywords: *carbon fiber, intercalation, swelling, micro-cracking, fracture mechanics*

1 Introduction

One of the materials with a potential for use as electrode in lithium-ion batteries is carbon fiber. In future structural batteries these carbon fibers will also have a load bearing function. Fiber degradation may also affect the ion diffusivity and the number of charge-discharge cycles with high energy efficiency. To ensure the mechanical durability of this type of batteries mechanical degradation mechanisms in fibers during service life have to be analyzed to develop guidelines for material selection.

Lithium ion intercalation/deintercalation in carbon fiber is a transient process causing non-uniform swelling of the carbon fiber electrode. The gradients of lithium ion distribution lead to formation of mechanical stresses in the fiber. During deintercalation these stresses may lead to initiation and growth of radial cracks in the fiber. In intercalation arc-shaped cracks deviating from the tip of the radial cracks may form. Micro-crack formation decreases the mechanical properties of the fibers and reduces the charging properties of the battery due to decreased diffusivity. The crack propagation and possible damage evolution scenarios were analyzed using linear elastic fracture mechanics. Finite element method (FEM) calculations were performed for stress and fracture mechanics calculations.

2 Theoretical Background

2.1 Ion Concentration in Carbon Fiber

We consider an infinite electrolyte with uniformly distributed carbon fibers. This system can be represented by a cylindrical unit cell with a long fiber surrounded by an electrolyte. During the intercalation lithium ions diffuse into the fiber and their distribution along the radial coordinate can be described by concentration distribution, which follows diffusion equation.

$$\partial C / \partial t = D \Delta C \qquad (1)$$

where C is relative ion concentration in the fiber with respect to available sites, Δ is the Laplace operator and D is diffusion coefficient. In the particular case of a long fiber the diffusion is in-plane and the concentration is a function of fiber radial and angular coordinates r and θ respectively. Therefore

$$\Delta = \frac{1}{r}\frac{\partial}{\partial r}\left(r\frac{\partial}{\partial r}\right)+\frac{1}{r^2}\frac{\partial^2}{\partial \theta^2} \qquad (2)$$

Boundary condition at the fiber surface ($r = r_f$) [1] is:

$$Dc\nabla C + (k_a^{'} + k_c^{'})(C - C_R) = 0 \qquad (3)$$

where $k_a^{'}$, $k_c^{'}$ are anodic and cathodic rate constants, Parameter C_R has a meaning of saturation concentration of ions in the fiber.

In the present study the focus is on mechanical stresses therefore all unknown electrochemical parameters are reduced to one unknown parameter B (the Biot constant). Thus, varying this parameter from zero to infinity we cover all possible combinations of parameters such as diffusion coefficient, cathodic and anodic rate constants, etc. We use definition and notation of electrochemical parameters as in [1,2] .

2.2 Stress Distribution in Carbon Fiber

In the considered loading case all shear stress components are zero. We obtain generalized plane strain $\varepsilon_z = const$ solution (z is axial coordinate). Stress–strain relationships for transversally isotropic fiber (indices 1,2 and 3 correspond to r, θ and z directions) are obtained:

$$\varepsilon_r - \beta_1 c_0 C = -\frac{\nu_{31}}{E_3}\sigma_z + \frac{1}{E_1}\sigma_r - \frac{\nu_{12}}{E_1}\sigma_\theta \qquad (4)$$

$$\varepsilon_\theta - \beta_1 c_0 C = -\frac{\nu_{31}}{E_3}\sigma_z + \frac{1}{E_1}\sigma_\theta - \frac{\nu_{12}}{E_1}\sigma_r \qquad (5)$$

$$\varepsilon_z - \beta_3 c_0 C = +\frac{1}{E_3}\sigma_z - \frac{\nu_{31}}{E_1}\sigma_r - \frac{\nu_{31}}{E_1}\sigma_\theta \qquad (6)$$

In (4)-(6) β_i, $i = r, \theta, z$ are the swelling coefficients in the main fiber directions, c_0 is the maximum concentration of the ions, when all possible sites are occupied. The diffusion problem and the elastic problem are decoupled. We can first find the concentration distribution using boundary conditions. The concentration distribution does not depend on the elastic stress state. The concentration distribution $C(r, \theta, \tau)$ is used as an input in the elastic problem, which can be solved at any arbitrary instant of τ, where τ is normalized time defined as

$$\tau = \frac{tD}{r_f^2} \qquad (7)$$

The mathematical description of the concentration distribution is the same as for heat conduction problem with convection boundary conditions: parameter B has the meaning of the heat–transfer coefficient, C is analogous to the temperature distribution and C_R is the value of temperature in the surrounding medium. This analogy can be used to employ commercial finite element (FE) code ANSYS [3] in the presented paper) to find concentration and stress distribution.

3 FEM Model

3.1 Model and the Calculation Procedure

FEM models for stress distribution (no micro-cracks) analysis and for radial and arc-shaped crack growth analysis were generated. In all cases transient ion concentration and corresponding mechanical stress distributions were calculated. FEM software code ANSYS version 13.0 [3] was used to perform all calculations. Two phase (carbon fiber and matrix electrolyte) models were generated. First a FEM model for case without damage was generated. Taking the advantage of the symmetry of the problem, only ¼ of the total transverse FEM model is needed to perform calculations. Two cases were analyzed: Case 1 with the Biot constant B=500 and Case 2 with B=5. The relation between diffusion coefficients for Cases 1 and 2 is then the following: $D_1 = 0.01 D_2$.

To analyze the radial crack growth FEM model shown in Fig.1 was generated. According to the discussion in the Introduction, the first damage in the fiber may be in a form of radial cracks forming at the surface of the fiber. In Fig. 1 l_r is the radial crack length. The crack face position corresponds to the angular coordinate of $\theta = \pi/4$. Due to the symmetry conditions on the horizontal and on the vertical axis the fiber in this model has four cracks. Interaction between them was not investigated in this study. Mesh refinement was used in vicinity of the crack tip as shown in the detail in Fig.1. The representation of the crack geometry in Fig.1b is schematic and it illustrates the deformed state. Since the ion diffusion is in the radial direction, the diffusion is not affected by the presence of the radial crack. When solving the elastic problem contact elements were generated on the crack surfaces to prevent mechanical interpenetration. The energy release rate was calculated using the J-integral based routine implemented in ANSYS version 13.0 [3].

Following the scenario previously described in the Introduction, arc cracks may deflect from the radial cracks. The FEM model for arc crack growth analysis is shown in Fig.2.

As shown in the detail in Fig.2b the length of the previously formed radial crack is l_r, its angular coordinate is $\theta = \pi/4$, while l_θ is the arc length of the arc crack, which is assumed to grow in circumferential manner along the arc with radius ($r_f - l_r$), symmetrically with respect to the radial crack. Due to applied symmetry conditions the

model corresponds to four radial cracks with arc branches. As in Fig. 1b, also in Fig. 2b the representation of the crack geometry is schematic and illustrates the deformed state. Contact elements were generated on all crack surfaces including the initial radial crack surface to prevent interpenetration.

As in the case of radial cracks the calculation of the energy release rate for arc cracks was performed using the J-integral based routine implemented in ANSYS.

The elastic properties of the carbon fiber used in this study are given in Table 1. The elastic modulus of the isotropic matrix was $E_m = 1$ MPa, the Poisson's ratio of matrix was $\nu_m = 0.3$.

In [4] the swelling strain $\beta_3^f c_0 C_R$ of approximately 0.3% was experimentally determined and it corresponded to measured capacity of 135 mAh/g at 1 hour charge. In [5] it was shown that for PAN based IMS65 carbon fiber electrodes the capacity can be increased by up to 3 times, when charging slower, meaning that more lithium ions can be intercalated leading to higher swelling. Thus, based on these values, the longitudinal swelling strain was assumed $\beta_3^f c_0 C_R$ = 0.9% to account for 3 times higher axial swelling. Swelling strain in transversal direction was assumed $\beta_1^f c_0 C_R$ =1.0%. Although atomic scale experimental data for expansion of interlayer distance in carbon fibers due to lithium ion intercalation are available (see for example [6] using X-Ray diffraction), the macroscopic transverse swelling coefficient for carbon fibers has not yet been presented in the literature.

Nevertheless, it has to be realized that in the considered linear problem the actual value of the swelling coefficient is not affecting conclusions: increasing the value *n* times will lead to *n* times increase of stresses and strains and to n^2 increase of strain energy release rate.

4 Results and Discussion

4.1 Stress Distribution Results

Results are presented for different time instances t^* as will be explained below. *x* is the radial coordinate (*x=0*) is in the fiber center.

In Figures 3a,b and 4a,b distributions of ion concentration C, radial stress σ_r, tangential stress σ_θ and axial stress σ_z are presented for Cases 1 and 2 respectively. The results in Figures 3a,b and 4a,b are presented in the same time scale units and are directly comparable: the various instants of the normalized time are calculated as $t^* = \tau_{1,i} = 0.01\tau_{2,i}$, where i denotes intercalation.

At fixed time instants the concentration distribution for the Case 1 (Fig.3a,b) has higher gradients than for the Case 2 (Fig.4a,b) because the diffusion coefficient for the Case 2 is 100 times higher than for the Case 1 and the diffusion is much faster. The higher gradients in concentration result in higher values of the stress components in Case 1 (Fig.3a,b) compared to Case 2 (Fig.4a,b). For undamaged fiber the concentration profiles and stress distributions coincide with the analytical series expansion solution presented in [1]. During intercalation the radial stress is positive with the maximum at the fiber axis. It seems from Fig. 3a,b and 4a,b that the maximum values of are slightly higher for Case 1 (with B =500). This result should, however, be treated with a caution because the shown time instants were not selected to present the stress maximum. In the central region the hoop stress values are similar to the radial stress values. In the interface region they are almost two times higher but they are compressive. Hence, the only damage mode that could be expected to initiate in the intercalation phase is cracks in the central region because of combined action of radial and hoop stresses. The values of these stresses are relatively low and the probability of this damage mode as compared with other possibilities described below is low.

The extremely high compressive axial stresses in Figures 3b and 4b are due to the applied constraint of the plane strain condition that was used in calculations. Fig.5 proves that the conditions at the fiber ends (plane strain or generalized plane strain condition) do not influence the radial and tangential stress distributions.

Results presented in Fig. 3 and 4 correspond to intercalation. During deintercalation (assuming $C_R = 0$) the initial concentration distribution is uniform with $C = 1$, lithium ions start to leave the interface region and the final value of the concentration is zero. The concentration distribution dependence on time for this process can

be obtained from data in Fig.3 and Fig.4 by creating a mirror picture with respect to the axis $C=1$ and shifting the result by one unit down in the vertical direction. The stresses distributions in Fig.3 and Fig.4 are just changing sign.

Hence, the high hoop stresses σ_θ become positive and since they are roughly two times higher than the tensile radial stress during intercalation, we can expect that the first damage event will take place during the deintercalation. The damage mode will be radial crack under Mode I conditions (due to assumed symmetry).

The possible effect of the electrolyte elastic properties on the stress distributions and on the presented conclusions was investigated by changing the elastic modulus of the surrounding electrolyte from 1 MPa to 100 MPa. The only noticeable relative stress change was for the radial component at the interface: from being negligible it became small. Since it does not influence the stress distribution and the sequence of events in any noticeable way, in following calculations the value E_m =1 MPa was used.

4.2 Radial Crack Growth

The concentration distributions obtained from the FEM model with radial cracks (Fig.1) are identical to distributions from a FEM model with the undamaged fiber. It is due to the geometry of the model and the used boundary conditions which govern that the flux has only the radial component; therefore radial cracks do not interrupt the ion flow.

The conditions for the radial crack growth were analyzed using the model described in Section 3. Results are presented for Case 1 only (B =500). Fig.6 shows Mode I energy release rate G in J/m^2 for radial crack growth during deintercalation. The presented results were obtained taking the fiber radius r_f =1μm. The curves in Fig.6 each correspond to normalized time $t^* = \tau_{1,d}$, where d denotes deintercalation. According to results plotted in Fig.6a in the beginning of deintercalation the G curves are monotonously decreasing with the radial crack length l_r . One can visualize the presented curves as evolution of one curve which is changing its values and shape with the time.

In the beginning ($t^* \le 2.5$) this curve has growing values in increasing time instants, after that the values at the same l_r are decreasing. If the radial crack would grow in a quasi-static manner based on criterion $G = G_c$ with a constant G_c, the description of events is as follows. Assuming a certain initial crack length l_r^0, see Fig.6a, this crack will start to grow at the time instant when the G curve corresponding to the reached concentration distribution crosses the horizontal G_c curve in the point $l_r = l_r^0$. Since in this part of the deintercalation the G curve is growing with time the cross-point with G_c curve is moving with the time to the right, which means that the radial crack is growing. As described above, after reaching $t^* \approx 2.5$ the G curve starts to decrease, which means that the cross-point is moving to the left. This means that the value for the reached crack length is lower than G_c and the crack growth stops. It will not grow further in the following intercalation-deintercalation cycles. This behavior is schematically shown in Fig.7a.

If the G_c value is very high, the G curve will never cross the G_c curve and the radial defect will never grow in a quasi-static manner. However, in this case the radial crack can grow during the many applied cycles of charging and discharging as the result of fatigue, which may be governed by power law. Since this process is related to the change of the strain energy release rate ΔG , it can be better described using Fig.6b. The ΔG during one cycle is different for each crack length. It is calculated as the difference between the maximum and the minimum (which is zero) in the G curve in Fig.6b. According to power law the ΔG value determines the rate of the crack growth. For short radial crack, ΔG is large and the crack growth rate with the number of deintercalation cycles will be high. With increasing radial crack length ΔG reduces and the growth rate, $l_r^{\bullet}$, will slow down and eventually stop (the values at $l_r = 0.7$ in Fig.6a,b are close to zero). This behavior is illustrated in Fig.7b.

Results in Fig.6a,b correspond to deintercalation. During intercalation if the radial crack is short the tangential stresses, σ_θ at the crack tip are compressive (see Fig.3b). For longer crack lengths it is expected that the tangential stresses σ_θ at the crack tip will be tensile and the crack may propagate further in radial direction in Mode I. However, considering that in the outer region a large part of

the radial crack would be closed (based on the tangential stress distribution in Fig.3b) and only the region close to the crack tip would be open, we can presume that the energy release rate values will be much smaller than those shown in Fig.6. Trial numerical calculations confirmed this result. Therefore, in the first approximation the contribution of the intercalation cycle on the radial crack growth in quasi-static and also in fatigue case can be neglected.

4.3 Arc Crack Growth

Numerical results presented in this section are for Case 1 only (B=500). The results described in the previous section showed that the driving force for radial crack growth decays with the crack length l_r. When G for radial crack growth becomes too small, crack deflection in the tangential direction can take place due to tensile radial stresses during the intercalation. Certainly, the strain energy release rate for the radial crack growth and for growth of the arc crack developing from the tip of the radial crack can be very different. In addition, the radial crack growth is expected during deintercalation whereas the arc crack may grow during the intercalation. Furthermore, in an anisotropic fiber with certain morphology of graphitic sheets the G_c for crack propagation in the tangential direction and in the radial direction may be very different. This material property for transverse directions in the fiber has not been measured. The same is the situation regarding the fatigue parameters. Therefore the presented results can be useful in discussions regarding the possible damage modes but at present they cannot be used to predict the real damage behavior of particular type of fibers.

While in the presence of radial cracks the concentration distribution is identical to that of undamaged fiber, this no longer applies for the case of arc cracks deflecting from radial cracks. According to the model geometry the arc cracks are perpendicular to the direction of flow.

They "shield" the inner regions (the flux over the crack surfaces is zero) and the concentration distribution is no longer axisymmetric. Thus the concentration distribution depends strictly on the length l_θ and the radial coordinate $(1-l_r)$ of the arc crack. Fig.8 shows a comparison between the axisymmetric concentration distribution along the radial coordinate obtained for undamaged fiber (or fiber with radial cracks only) and the concentration distribution in the case when the arc crack is present. Comparison in Fig.8 is performed at the normalized time $t^*=25$, the length of the arc crack is $l_\theta=0.7(\pi/2)(1-l_r)$, where the length of the radial crack is l_r=0.3 (see Fig.2 for reference).

Two curves in Fig.8 show the concentration distribution along x at two values of the angular coordinate θ=0° and θ=45°. It can be concluded that due to the shielding effect of the arc crack, at θ=45° the ion concentration on the outer side of the arc crack is approaching the saturation level whereas on the inner side the concentration is much lower (the concentration increases due to diffusion in the hoop direction only). On the line θ=0° the radial distribution is lower than in the axi-symmetric case because part of the ions have to leave the radial path to move into the shielded region.

Due to dependency of the concentration distribution on the geometry of the radial and arc cracks, the energy release rate calculations were performed for a range of different combinations of l_r and l_θ. G calculation results given in Figures 9, 10 and 11 correspond to three cases of the radial crack length: $l_r=0.1$, $l_r=0.3$ and $l_r=0.7$ respectively, $r_f=1$. The results are plotted with respect to the normalized length of the arc crack $l_{\theta n}=l_\theta/\left((\pi/2)(1-l_r)\right)$, where $(\pi/2)(1-l_r)$ is the maximal possible arc length at this distance from the fiber center. It can be seen that for a case, when the initial radial crack length is $l_r=0.1$, distinct maximum can be observed (Fig.9a), when plotting G as a function of the arc crack length $l_{\theta n}$. This means that the arc crack propagation in quasi-static mode would be rather stable. On the other hand, for cases when $l_r=0.3$ (Fig.10) and $l_r=0.7$ (Fig.11) monotonously increases with the arc crack length indicating an unstable propagation.

More detailed description of the crack propagation process can be performed similarly as it was done for radial crack growth: selecting certain value of G_c and the initial arc crack length $l^0_{\theta n}$. These values are shown in Fig. 9a, since this will be the case discussed.

When the intercalation starts the G curve in Fig. 9a "grows" in the vertical direction until it eventually

crosses the G_c line at $l_{\theta n}^0$. If it happens the arc crack starts to grow, the G to the right of the cross-point is higher than in the cross-point and the crack growth is unstable. Since the time scale of the crack growth is much smaller than the time scale for diffusion, we can consider that the arc crack grows instantaneously at fixed concentration (t^*). The crack stops, when its size corresponds to the second cross-point of the G_c line and the G curve. After that the arc crack can still grow if the G curve is still rising above G_c as a result of concentration redistribution with time. For arc cracks corresponding to longer radial cracks, Fig. 10 and Fig.11, there is no maximum in the G curve and therefore there is no second cross-point. If the arc crack starts to grow, the growth would be unstable until it connects with the other arc cracks symmetrically approaching from the neighboring parts of the fiber. However, if the arc crack is not long, the values of the G for these cases are slightly lower than in Fig. 9 and it may be more difficult to start the arc crack propagation.

Behavior in fatigue during many intercalation cycles may be analyzed using Fig.9b. For an arc crack generated by short radial crack in the beginning the ΔG is small and the arc crack growth rate, $l_{\theta n}^{\bullet}$, is low. It increases with the increase of the arc crack length, reaches maximum and slows down approaching to zero. For cases when the arc crack originates from longer radial cracks, the ΔG and also the crack growth rate increases with time (accelerated unstable growth). These trends are schematically shown in Fig.12a and 12 b.

Comparing the values obtained for deintercalation with the values for intercalation shown in Fig.9-11 it was concluded that G in deintercalation is negligible and cannot significantly contribute to the arc crack growth.

Since the axial symmetry in ion concentration and stress distributions is lost, if the arc cracks are present, Mode II propagation should also be considered. However, trial calculations using virtual crack closure technique [7] showed that even though Mode II is present, the magnitude of G_{II} compared to magnitude of G_I is negligible.

5 Conclusions

Lithium ion diffusion in a carbon fiber was analyzed numerically with the aim to understand and to evaluate possible damage mechanisms (crack formation and growth) in the fiber as the result of nonuniform swelling. Thermal analogy with ion diffusion in combination with FEM based elastic stress analysis was used.

Simple analysis of transient ion concentration distributions and corresponding stress distributions showed that radial cracks may appear in the fiber during the deintercalation. During the following intercalation arc cracks may deflect from the previously formed radial cracks. Growth of these two types of cracks was analyzed using fracture mechanics approach.

During the first deintercalation high hoop stresses can initiate radial crack growth in the fiber. The crack growth with time is stable. It stops when due to ion concentration gradient change with time the strain energy release rate starts to decrease.

The radial crack can also grow in fatigue with increasing number of intercalation-deintercalation cycles. The fatigue crack growth rate is highest, when the crack is short and becomes equal to zero when the radial crack length is about 70% of the fiber radius.

During intercalation the arc crack may deflect from the tip of the radial crack. Its growth in a quasi-static manner becomes unstable as soon as the critical value of the strain energy release rate is reached. However, the arc crack growth stops if the arc crack has originated from a relatively short radial crack. In fatigue the behavior depends on the length of the radial crack, from which the arc crack deflected. If the radial crack was short, the arc crack will first grow with an increasing rate. The rate will reach maximum, then it will be reduced and the growth will eventually stop before the arc crack goes around the whole fiber. If the radial crack from which the arc crack starts is large, the arc crack propagates in fatigue with increasing growth rate until it eventually links with other arc cracks coming from other radial cracks.

6 Acknowledgement

Funding by the Swedish Foundation for Strategic Research (SSF), framework grant RMA08-0002 is gratefully acknowledged.

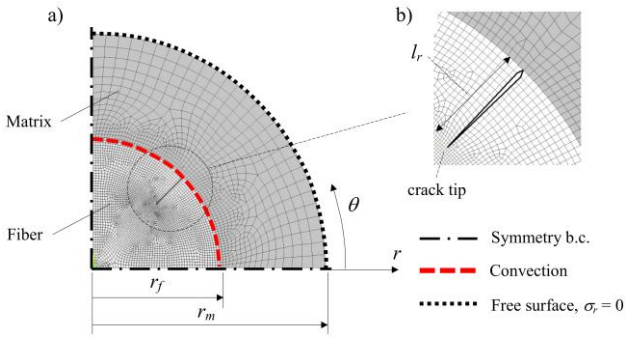

Fig. 1. FEM model for radial crack growth analysis

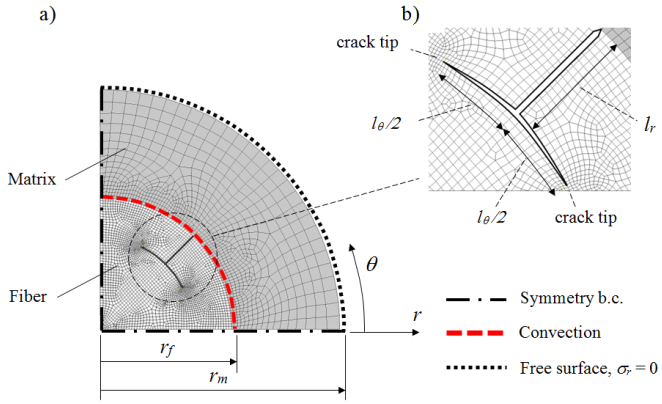

Fig. 2. FEM model for arc-shape crack growth analysis

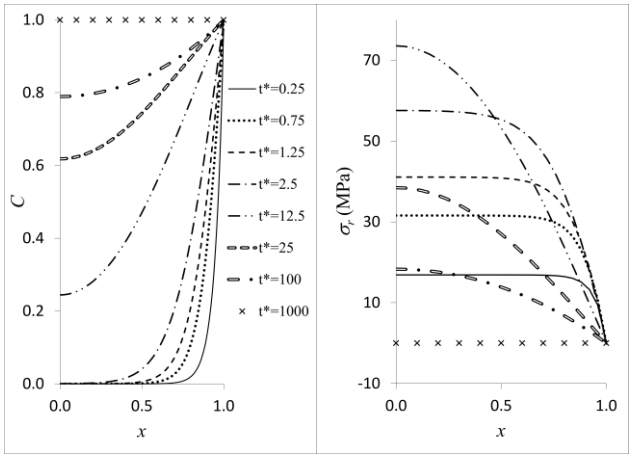

Fig. 3a. Distribution of ion concentration and radial stresses. $B = 500$

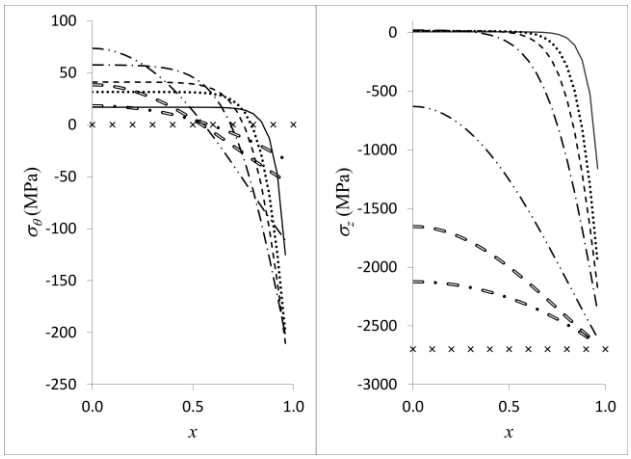

Fig. 3b. Distribution of corresponding tangential and axial stresses. $B = 500$

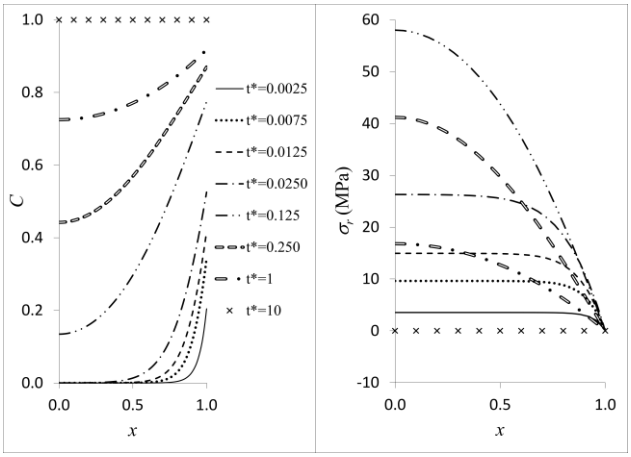

Fig. 4a. Distribution of ion concentration and radial stresses. $B = 5$

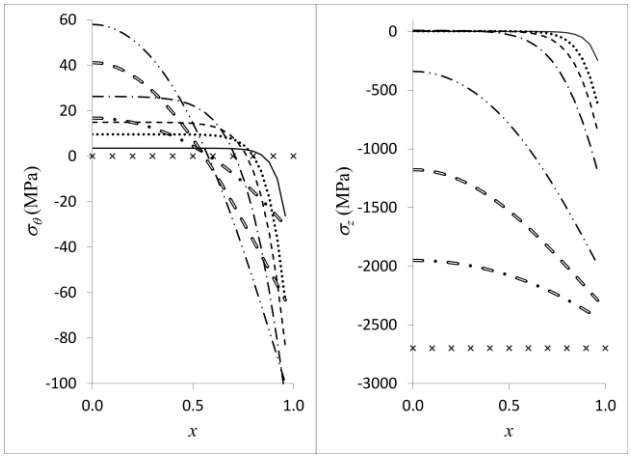

Fig. 4b. Distribution of corresponding tangential and axial stresses. $B = 5$

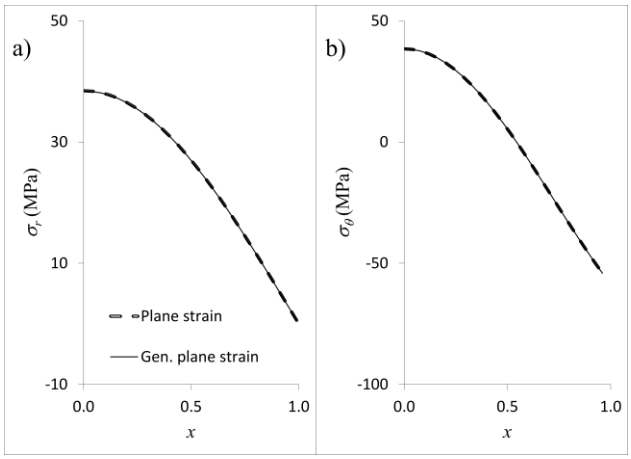

Fig. 5. a) Radial stress distribution and b) tangential stress distributions at plane strain and generalized plane strain conditions.

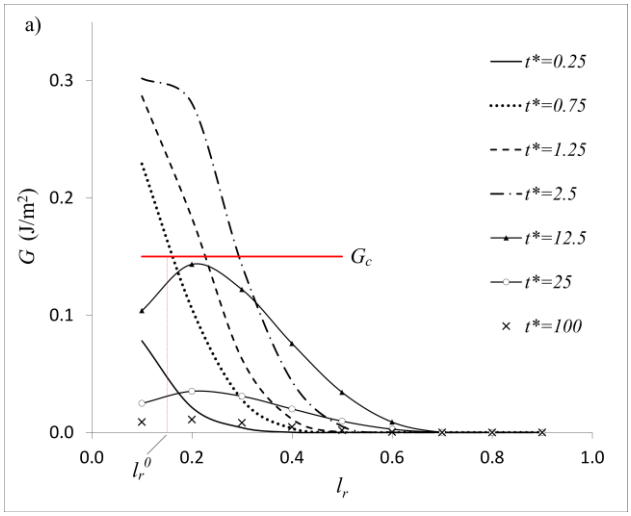

Fig. 6a. Energy release rate for radial crack growth during deintercalation for Case 1.

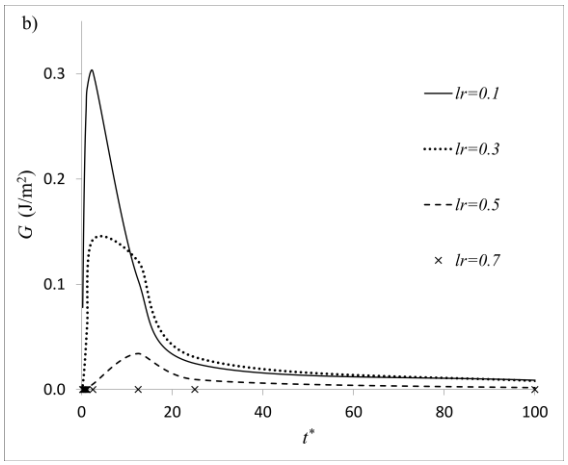

Fig. 6b. Energy release rate for radial crack growth during deintercalation for Case 1.

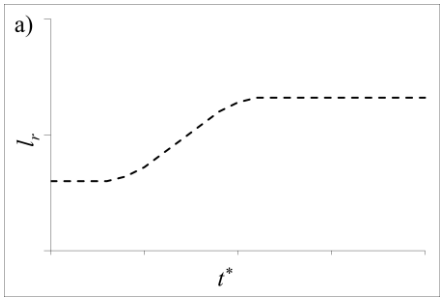

Fig. 7a. Schematic showing of radial crack propagation length in quasi-static manner

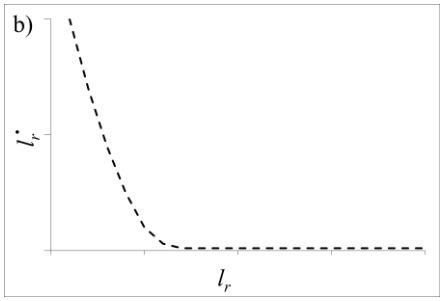

Fig. 7b. Schematic showing of radial crack propagation rate $l_r^\bullet$ in cyclic loading

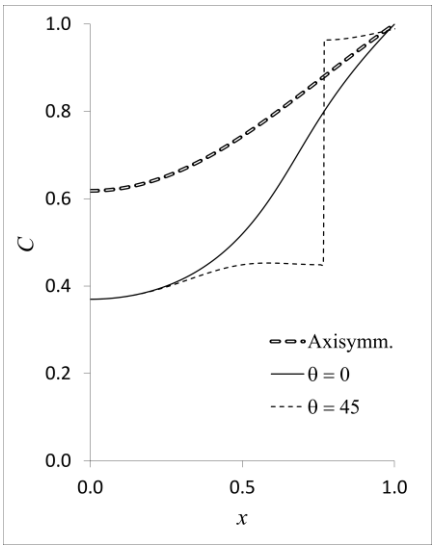

Fig. 8. Concentration distribution at intercalation time t^*=25 in carbon fiber with radial and arc cracks, l_r =0.3, $l_\theta = 0.7(\pi/2(1-l_r))$

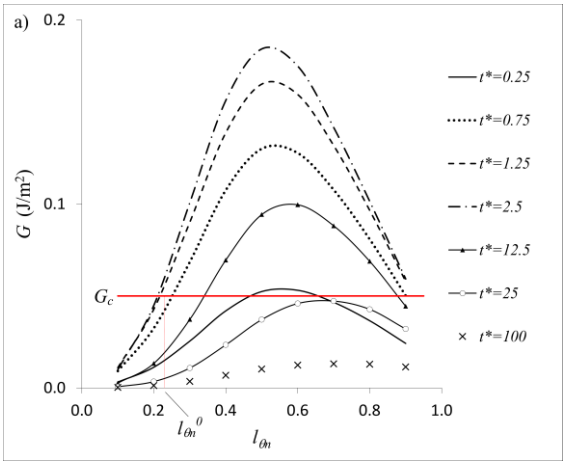

Fig. 9a. Energy release rate for arc crack growth during intercalation. l_r =0.1.

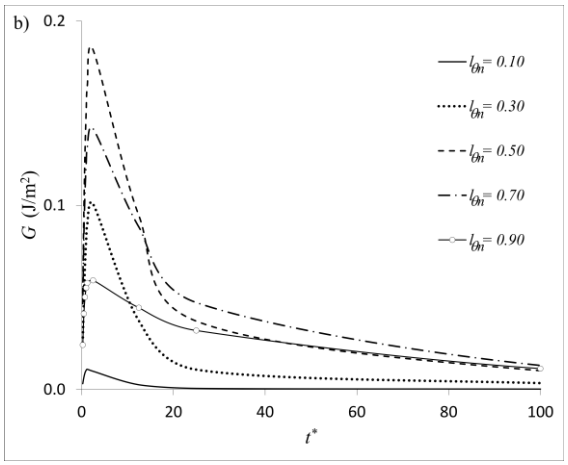

Fig. 9b. Energy release rate for arc crack growth during intercalation. l_r =0.1.

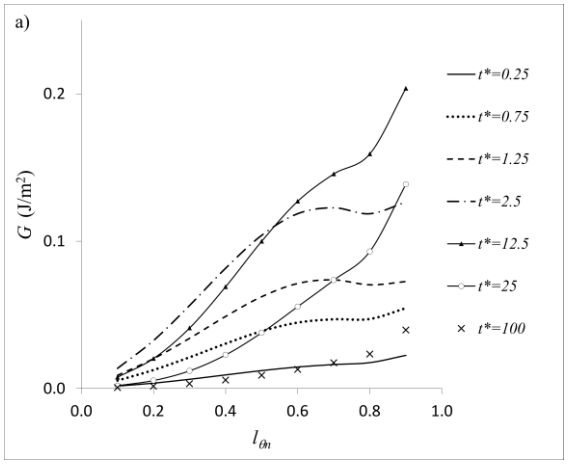

Fig. 10. Energy release rate for arc crack growth during intercalation. l_r =0.3.

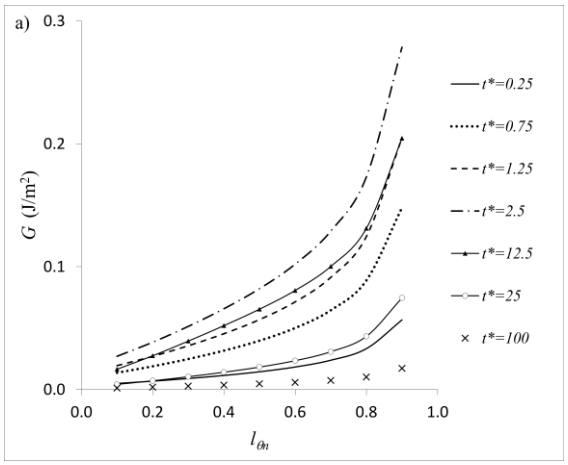

Fig. 11. Energy release rate for arc crack growth during intercalation. l_r =0.7.

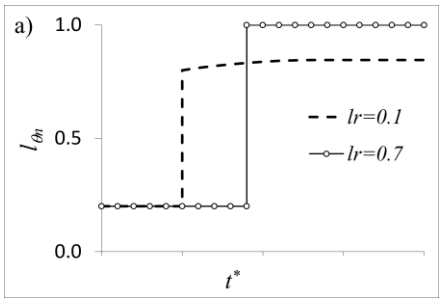

Fig. 12a. Schematic showing of arc crack propagation length in quasi-static manner.

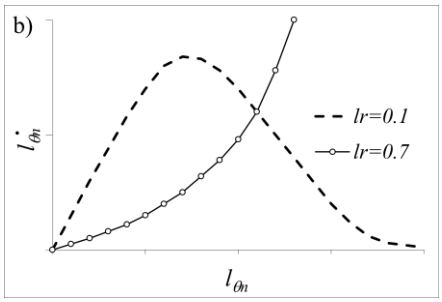

Fig. 12b. Schematic showing of arc crack propagation rate $\dot{l}_{\theta n}$ in cyclic loading.

Table 1. Elastic properties of the carbon fiber

E_3^f	E_1^f	G_{31}^f	ν_{31}^f	ν_{12}^f
[GPa]	[GPa]	[GPa]	[-]	[-]
300	30	20	0.2	0.45

References

[1] Y.T. Cheng and M.W. Verbrugge "Diffusion-induced stress, interfacial charge transfer, and criteria for avoiding crack initiation of electrode particles". *Journal of the Electrochemical Society*, Vol. 157, No. 4, pp 508-516, 2010.

[2] M.W. Verbrugge and B.J. Koch "Modeling lithium intercalation of single-fiber carbon microelectrodes". *Journal of the Electrochemical Society*, Vol. 143, No. 2, pp 600-608, 1996.

[3] ANSYS Academic Research, Release 13.0, Canonsburg, Pennsylvania, 2011.

[4] E. Jacques, M.H. Kjell, D.Zenkert, G. Lindbergh and M. Behm "Expansion of carbon fibres induced by lithium intercalation for structural electrode applications". *Carbon*, In Press, 2013.

[5] M.H. Kjell, E. Jacques, D. Zenkert, M. Behm and G. Lindbergh "PAN-based carbon fiber negative electrodes for structural lithium-ion batteries". *Journal of the Electrochemical Society*, vol.158, No. 12, pp 1455-1460, 2011.

[6] N. Imanishi, K. Kumai, H. Kokugan, O. Takeda and O. Yamamoto "Li-NMR study of carbon fiber and graphite anodes for lithium ion batteries". *Solid State Ionics*, Vol. 107, pp 135-144, 1998.

[7] G.R. Irwin "*Fracture, Handbuch der Physik*". Springer Verlag, Berlin, vol.5, 1958.